# Title: Evolocumab as an immunomodulator in glioma: A window of opportunity trial evaluating PCSK9 inhibition to enhance surface MHC-I on tumor

**Authors:** Kirit Singh[1,2], Matthew W. Foster[3], Marlene J. Violette[3], Kelly M. Hotchkiss[1,2], Chelsea O. Railton[1,2], Emily E. Blandford[1,2], Kathryn E. Blethen[1,2], Elizabeth L. Thomas[1,4], David M. Ashley[1], Annick Desjardins[1], Henry S. Friedman[1], Margaret O. Johnson[1], Allan Friedman[1,2], Stephen Keir[1], Evan D. Buckley[6], James E. Herndon[5, 6], Roger E. McLendon[1, 4], John H. Sampson[1,2], Evan Calabrese[7], Giselle Y. Lopez[1, 2, 4], Gerald A. Grant[1,2], Anoop P. Patel[1,2], Chuan-Yuan Li[8], Peter E. Fecci[1,2†], Mustafa Khasraw[1,2†*]

**Affiliations:**
[1]The Preston Robert Tisch Brain Tumor Center at Duke University; Durham, NC, US.
[2]Department of Neurosurgery, Duke University; Durham NC, US.
[3]Duke Proteomics and Metabolomics Core Facility, Duke University; Durham, NC, US.
[4]Department of Pathology, Duke University; Durham, NC, US.
[5]Department of Biostatistics and Bioinformatics, Duke University; Durham, NC, US.
[6]Duke Cancer Institute Biostatistics, Duke University; Durham NC, US.
[7]Department of Radiology, Duke University; Durham, NC, US.
[8]Adjunct Professor in the Department of Dermatology, Duke University; Durham, NC, US.

[†]These authors contributed equally to the manuscript.

***Corresponding Author.** Mustafa Khasraw, MD, The Preston Robert Tisch Brain Tumor Center, Duke University | Box 3624, Durham, NC 27710, T +1 919.684.6173 | F +1 919.681.1697, mustafa.khasraw@duke.edu

**Abstract:** Many cancers, including glioma, evade immunosurveillance by downregulating surface major histocompatibility class (MHC)-I. Proprotein convertase subtilisin/kexin type 9 (PCSK9) promotes degradation of multiple receptors, including MHC-I and peripheral levels are specifically elevated in glioma (Human Protein Atlas). Inhibition of PCSK9 (PCSK9i) blocks MHC-I degradation. Evolocumab is a PCSK9i monoclonal antibody (mAb) indicated for hyperlipidemia. However, mAbs have limited penetrance across the blood brain/tumor barrier (BBB/BTB). We conducted a non-randomized surgical window-of-opportunity study to evaluate if peripheral evolocumab penetrates the BBB/BTB and effects tumor (PesKE; NCT04937413). 32 patients with newly diagnosed or recurrent glioma were enrolled (M: 16, F: 16; average age of controls: 51.85, evolocumab: 53). Of these, 4 who received evolocumab and 17 control participants had tissue for research. No significant adverse events were reported. However, BBB/BTB penetration (assessed by mass spectroscopy (LC-MS/MS)) was akin to other mAbs, with a tumor:blood ratio of 0.0332 (SD±0.0215) in contrast-enhancing and 0.0112 (SD±0.0039) in non-contrast-enhancing cases. LC-MS/MS analysis of the tumor proteome found a positive, but non-significant, relationship between evolocumab and MHC-I (HLA-A ($R^2$=0.5002, p=0.2928), HLA-B ($R^2$=0.7269, p=0.1474)). A significant negative relationship was observed between tumoral evolocumab and Apolipoprotein E ($R^2$=0.9113, p=0.0454*). Tumor tissue with the highest evolocumab demonstrated increased surface MHC-I and $CD8^+$ T cell infiltration (assessed by immunofluorescence and immunohistochemistry). In conclusion, pre-resection evolocumab is well tolerated but exhibits BBB/BTB penetrance akin to other mAbs. However, increased tumoral evolocumab/PCSK9i may enhance MHC-I/$CD8^+$ infiltration and reduce ApoE. Future work will explore combining evolocumab with BBB/BTB opening therapies like low-intensity focused ultrasound.

**One Sentence Summary:** We conducted a tissue-based study in glioma patients to evaluate if peripheral evolocumab enters brain, enhances MHC-I expression, and boosts $CD8^+$ T cell tumor infiltration.

# Main Text:

## INTRODUCTION

Tumoral evasion of the immune system is a key driver of resistance to immunotherapy. One such method of evasion is downregulation of surface major histocompatibility complex class I (MHC-I) (*1*). Absence of MHC-I on the cell surface restricts neoantigen presentation and hides tumor from cytotoxic $CD8^+$ T cells. This phenomenon has been observed in many cancers, including primary brain malignancies like glioma (*2*). Loss of MHC-I results in an immunologically cold tumor, with few tumor-infiltrating lymphocytes (TILs) (*3*) and worsened clinical outcomes (*4*). While recent findings by our group demonstrate that $CD8^+$ killing can occur independently of MHC-I via the NKG2D-NKG2DL axis (*5*), such killing depends on prior T cell priming via T cell receptor (TCR) activation. Restoring MHC-I expression may therefore also facilitate this priming of $CD8^+$ T cells, thereby enabling them to kill tumor (*6, 7*).

*Liu et al* found that regulators of cholesterol metabolism (*8*) such as proprotein convertase subtilisin/kexin type 9 (PCSK9) also influence the recycling of MHC-I receptors between the plasma membrane and cytoplasm (*9*). PCSK9 was initially developed as a drug target for hypercholesteremia as it was first understood to promote degradation of the low-density lipoprotein receptor (LDL-R) (*10*). However, this effect has been found to translate across multiple surface receptors, including the very low-density lipoprotein receptor (VLDL-R), Apolipoprotein E receptor 2 (ApoER2) and cluster of differentiation 36 receptor (CD36) (*10, 11*). Similarly, *Liu et al* demonstrated that high levels of PCSK9 promote the internalization of MHC-I to intracellular lysosomes, wherein it is degraded (*12*). Deletion/inhibition of PCSK9 blocked this pathway and increased tumoral expression of MHC-I, enhancing infiltration of cytotoxic $CD8^+$ T cells (mechanism in **Fig. S1**). Analyses of gene expression databases finds that PCSK9 mRNA expression negatively correlates with cytotoxic lymphocyte markers (CD8A) in esophageal cancer, cervical squamous cell carcinoma, endocervical adenocarcinoma and pancreatic adenocarcinoma (*12*). When PCSK9 inhibition (PCSK9i) was combined with immune checkpoint blockade (ICB), such as anti-programmed-death 1 (αPD-1), enhanced anti-tumor efficacy in murine models of colon cancer and melanoma was observed (*12*). Interrogation of the pan-cancer cohort within the human protein atlas revealed that circulating plasma PCSK9 levels are increased in patients with glioma compared to other malignancies (**Fig. 1**) (*13*). We have previously outlined the need for combination immunotherapies to overcome the multiple resistance pathways that are present in high-grade glioma (*14*). Based on the findings by *Liu et al* and the elevated circulating levels of PCSK9 in glioma patients, we hypothesized that PCSK9i could reduce MHC-I degradation, thereby increasing MHC-I expression and enhancing recruitment of $CD8^+$ lymphocytes into tumor. PCSK9i could then be considered as part of a future combination approach with T cell dependent therapies like ICB.

This potential approach benefits from the commercial availability of PCSK9i therapies, which are approved by the Food and Drug Administration (FDA) for the management of hypercholesterolemia (*15, 16*). These include the monoclonal antibodies Alirocumab (*17*) and evolocumab (*18*) as well as the small interfering RNA (siRNA) Inclisliran (*19*). We selected evolocumab for evaluation as it had been used to demonstrate anti-tumor efficacy in combination with αPD-1 ICB in the above studies by *Liu et al.* Evolocumab also possesses useful pharmacokinetic (PK) characteristics for combination therapy. Evolocumab has a well-established safety profile, with the most common reported adverse event being mild injection-site reactions (*15*). Further, at the maximum dose of 420 mg, evolocumab rapidly decreased unbound PCSK9 in the periphery within 4 hours of administration and fully suppressed PCSK9 levels

up to 14 days following a single treatment (*20*). Phase 3 clinical trials of evolocumab found that over 2.2 years of follow-up, new binding antibodies developed in just 0.3% of treated participants, and none developed neutralizing antibodies to therapy (*16*).

As a monoclonal antibody (mAB), the ability of evolocumab to readily cross the blood-brain/tumor barrier (BBB/BTB) was uncertain (*21*). While the BBB/BTB may become disrupted in glioma (via surgery, radiotherapy, or disease progression) this results in heterogenous uptake for antibody-based constructs (*22*). Regions of tumor that are shielded behind non-disrupted regions of the BBB/BTB could therefore be left untreated (*23*). Despite this, evaluations of peripherally administered antibody therapy in the context of high-grade glioma (αPD-1) have demonstrated biological effect in the central nervous system (CNS) despite a cerebral-spinal fluid (CSF):serum ratio of just 0.009 (*24*). Further, evolocumab could associate with unbound PCSK9 in the periphery and prevent its downstream binding to tumor in the CNS, resulting in a similar pharmacodynamic (PD) effect.

Based on these data, we sought to determine whether evolocumab could affect the tumors of patients with glioma and increase surface MHC-I, with resultant infiltration of $CD8^+$ lymphocytes. To do so, we conducted a surgical window of opportunity (SWOOPP) study – The PCSK9i Inhibitor Evolocumab: A Surgical Trial of Pharmacodynamics and Kinetics Evaluation (PesKE, NCT04937413). Our objectives were to evaluate [1] whether evolocumab was detectable in intracranial glioma following subcutaneous administration, [2] the safety profile of evolocumab in the context of recurrent glioma, and [3] the downstream effects of PCSK9i on MHC-I expression/$CD8^+$ infiltration into glioma. We report summary findings from this trial and outline potential future combinatorial strategies using PCSK9 inhibition for intracranial malignancies.

## RESULTS

### Peripheral high-dose evolocumab is well tolerated in patients undergoing biopsy/resection of glioma

Between October 2021 and June 2023, a total of 32 adult participants (≥ 18 years old) with newly diagnosed or recurrent glioma consented to enroll on study (16M, 16F). All enrolled patients had a clinical indication for surgical resection, debulking or biopsy of their tumor. Participants were enrolled on to the treatment arm if it was feasible for them to receive evolocumab (420mg, subcutaneous) within 4-14 days before their planned procedure (trial design shown in **Fig. S2**). Of the 32 patients recruited to the study, 6 participants met inclusion criteria and consented to treatment with evolocumab (average age 53 (SD±19.88)), while 26 were assigned to the non-treatment group (average age 51.85 (SD±16.07). Full demographics and a breakdown of the diagnoses for both groups, including whether participants had newly diagnosed or recurrent glioma, is shown in **Table 1**). Tissue was taken for research analysis if excess was available beyond that required for diagnostic purposes.

Of participants enrolled in the treatment arm, 5 patients proceeded to surgical resection/biopsy of their tumor. One treatment patient was not able to proceed to surgical resection. Four of the 5 treated patients who underwent resection had both post-treatment blood and tumor tissue available for analysis. In the control arm, 17 participants had sufficient tissue and blood available for analysis (CONSORT (*25*) flowchart showing tissue distribution shown in **Fig. 2**). Time from treatment with evolocumab to tumor resection was 4.4 days on average (SD±1.5). Over the course of the study, no grade 3-5 adverse events (AEs) or serious adverse events (SAEs) were recorded. Of mild-moderate adverse events which were possibly, probably, or definitely related to evolocumab, the commonest were injection site reactions (n=2 (33%)). A summary of all adverse events recorded during this study is shown in **Table 2** with those possibly, probably, or definitely related to evolocumab shown in Table 3**.**

**Mass spectroscopic detection of evolocumab finds higher levels in contrast-enhancing tumors, but an overall BBB/BTB penetrance akin to other mAbs**

To detect evolocumab accurately and specifically in tumor, we analyzed tryptic digests of neat drug, or drug after spiking into pooled human plasma using liquid chromatography coupled to tandem mass spectrometry (LC-MS/MS). We selected three candidate "proteotypic" tryptic peptides based on uniqueness versus reference human proteomes (*26*) and validation using spiked pooled plasma. Evolocumab was quantified in whole blood via a targeted LC-MS/MS assay which used stable isotope-labeled (SIL) internal standard peptides and an external calibration curve (*27*). Using the peptide that gave best figures-of-merit (e.g. lowest limits of detection and quantification), evolocumab was below limit of detection in blood prior to treatment but was quantified in all intervention patients following administration of drug (**Fig. 3A**). Relative levels of evolocumab were further quantified in tumor. Variability in evolocumab detection in tumors was observed across treated subjects, with complete absence in control cases (**Fig. 3B**). Based on the average of the three evolocumab-derived peptides, higher detection of evolocumab in tumors was noted for both intervention case IDs 1004 and 1007 with lower detection in case IDs 1005 and 1008 (**Fig. 3C**).

Evaluation of pre-operative imaging and pathology for the two cases with lower evolocumab detection found that they were lower grade non-contrast enhancing tumors (ID 1005: grade III Oligodendroglioma, ID 1008: grade II Astrocytoma, average tumor:blood ratio 0.0112 (SD±0.0039), MRI sequences shown in **Fig. 4A-D**)). Conversely, cases with higher evolocumab detection were both grade IV glioblastomas, with evidence of contrast enhancement on magnetic-resonance imaging for both (MRI, average tumor:blood ratio of 0.0332 (SD±0.0215)). When evaluating BBB/BTB penetrance via tumor:blood ratios, we observed variation between both grade IV glioblastoma cases (**Fig. 3D**, ID: 1004 tumor:blood ratio of 0.0547 vs ID: 1007 tumor:blood ratio of 0.0117). We observed that the tumor tissue with the highest overall levels of intra-tumoral evolocumab had the highest overall levels of drug detected in the periphery (ID: 1007, **Fig. 3A**). However, the highest uptake ratio of evolocumab was observed in the intervention case with the greatest amount of contrast enhancement observed on MRI (ID: 1004. T1-post contrast MRI sequence shown in upper right quadrant of **Fig. 4C**). Nevertheless, overall uptake of evolocumab (average tumor:blood ratio across all cases of 0.0222 (SD±0.0190) was in keeping with other peripherally administered monoclonal antibodies (mAbs, aPD-1: 0.009 (*24*)).

**Glioma tissue with higher evolocumab uptake exhibits increased HLA-A and -B and decreased Apolipoprotein E in the tumor proteome**

We next wanted to evaluate the pharmacodynamics of evolocumab. We hypothesized that drug treatment would result in increased MHC-I levels in resected/biopsied tumor and first sought to validate that non-targeted LC-MS/MS would appropriately determine high or low MHC-I expression on glioma. To do so, we analyzed immortalized glioma lines that have been reported in the literature to express either high levels of MHC-I (U343MG, MHC-I$^{Hi}$) or lower levels of MHC-I (U87MG, MHC-I$^{Lo}$) (*28*). We first performed flow cytometric analysis to confirm differential MHC-I (HLA-ABC) expression on these two cell lines (**Fig. 5A**). Similar trends in relative levels of HLA-A, -B and -C proteins were quantified in the cell proteomes from tryptic digests by non-targeted proteomics, with higher levels observed in the MHC-I$^{Hi}$ U343MG versus MHC-I$^{Lo}$ U87MG line (**Fig. 5B**). These data validated the use of LC-MS/MS for quantification of relative MHC-I.

We next quantified the proteomes of tumor tissue from both control and treatment participants. Despite a similar time from treatment to resection and dose across all intervention cases, we observed variable HLA-A (**Fig. 4C**) and -B (**Fig. 4D**) levels whereas HLA-C (**Fig. 5E**) remained largely unchanged. Interestingly, the highest relative abundances of HLA-A, -B and -C (arrows) were observed in the treatment case with the highest levels of intratumoral evolocumab – case ID: 1007 (**Fig. 3C**). An analysis of the abundances of

intra-tumoral evolocumab versus HLA-A/B/C showed a positive but non-significant correlation of intratumoral evolocumab and HLA-A (**Fig. 5F,** $R^2$=0.5002, p=0.2928, n=4) as well as HLA-B (**Fig. 5G,** $R^2$=0.7269, p=0.1474, n=4). However, no trend was seen for intratumoral evolocumab versus HLA-C (**Fig. 5H,** $R^2$=0.05003, p=0.7763, n=4).

We also evaluated if increased evolocumab translated into increased effect on lipid pathways in the brain using relative abundances of Apolipoprotein E that were quantified in the tumor proteome (the major apolipoprotein regulating CNS lipid metabolism (*29*), ApoE). Since PCSK9 has been implicated in degradation of ApoE receptors, we hypothesized that evolocumab would prevent ApoE receptor degradation, resulting in decreased levels of ApoE. Accordingly, analysis of the case with highest levels of intratumoral evolocumab (ID: 1007) found the lowest levels of ApoE in tumor (**Fig. 5I**, technical repeats across batch analyses shown). Notably, a correlation analysis showed a significant negative trend between ApoE and intratumoral evolocumab (**Fig. 5J**, $R^2$=0.9113, p=0.0454*, n=4). However, interpretation of these data is restricted to the 4 intervention cases for which sufficient tissue was available for LC-MS/MS analysis.

**Increased $CD8^+$ T cell infiltration and MHC-I cell surface expression is observed in tumor tissue with the highest evolocumab detection**

Finally, we wanted to establish whether higher abundances of MHC-I translated into increased cell surface expression. To do so, we performed parallel immunofluorescence (IF) and immunohistochemistry (IHC) in tumor tissue with either lower (ID: 1008, grade II astrocytoma) or higher (ID: 1007, grade IV glioblastoma) evolocumab uptake in tumor. IF staining of tissue with lower evolocumab uptake revealed low MHC-I expression (**Fig. 6A**). Co-staining with Wheat Germ Agglutinin (a marker for cell membranes, WGA) similarly showed limited membranous expression of MHC-I in tumor tissue with lower evolocumab uptake. Tumor tissue with lower evolocumab uptake also demonstrated lower $CD8^+$ density compared to tissue with higher uptake (assessed via IHC, **Fig. 6B**, 1008: 0.9986 $CD8^+$ per $mm^2$ vs 1007: 13.9757 $CD8^+$ per $mm^2$).

IHC analysis of tumor tissue with higher intratumoral evolocumab demonstrated multiple separate areas of inflammatory infiltrate. Unblinded pathologist review noted that unlike the typical perivascular pattern observed in glioma, the inflammatory infiltrate appeared to be largely within the parenchyma, with focal parenchymal aggregates (**Fig. 6C**, $CD8^+$ infiltrate marked by arrows). Paired IF staining found greater MHC-I expression in tumor regions which co-localized with areas of $CD8^+$ infiltrate. Co-staining with WGA revealed overlapping expression of MHC-I and WGA, suggesting increased membranous expression of MHC-I in tumors with high evolocumab uptake. Again, this interpretation is limited to intervention patients where excess tissue for IHC/IF was available (i.e., 2 intervention cases).

**DISCUSSION**

Immunologically cold tumors like high-grade gliomas have proven resistant to immunotherapies such as immune checkpoint blockade (*30*). Loss of MHC-I has long been considered to be a key factor in resistance to immunotherapy, although recent findings by our group demonstrate that $CD8^+$ killing can occur independently of MHC-I via the NKG2D-NKG2DL axis (*5*). However, such killing depends on prior TCR activation, and restoring MHC-I expression may also facilitate this priming of $CD8^+$ anti-tumor activity.

We therefore performed a small-scale tissue-based trial to assess both the PK and PD of evolocumab in glioma – a drug that has been shown to increase MHC-I expression and potentiate ICB in other cancers *in vivo*. We find that although evolocumab appears to have BBB/BTB penetrance in keeping with other mAbs (which have not demonstrated efficacy against glioblastoma) (*24, 30*), tumor

tissues with the highest evolocumab detection appeared to have increased membranous MHC-I surface expression. Those regions of tumor with increased MHC-I expression corresponded to regions of parenchymal $CD8^+$ infiltration, an uncharacteristic finding in higher-grade gliomas (*31, 32*).

Similarly, we observed that as evolocumab levels in tumor increased, ApoE levels declined. This suggested that increased presence of PCSK9i in the brain may prevent degradation of surface membrane receptors like ApoER2. Beyond demonstrating a relationship between drug levels and biological effect, we also note that ApoE is over-expressed in multiple cancers (*33*), including glioblastoma and low-grade glioma (*34*) and has been shown to play a role in suppressing inflammatory signaling in the CNS (*35*). ApoE has also been demonstrated to polarize macrophages from an inflammatory M1 phenotype to the anti-inflammatory M2 phenotype (*36, 37*). Although our study could not distinguish whether increased immune infiltrate was directly due to increased MHC-I or decreased ApoE, it is also feasible that PCSK9i could have a dual effect in inflaming tumor. This would be of particular value in high-grade gliomas, where immunosuppressive tumor associated macrophages (TAMs) are abundant (*38*). Therapeutic targeting of ApoE and its isoforms are also an active area of investigation in Alzheimer's disease, with gene editing approaches and monoclonal antibodies under development (*39*). Our findings suggest that PCSK9i may also reflect a further approach to decreasing circulating levels of ApoE within the CNS and could possibly be considered in the context of neurodegenerative diseases like Alzheimer's. However, further determination of the biological significance of ApoE reduction in glioma is required, along with validation of evolocumab's effects on circulating ApoE levels in the CNS.

Despite this, our study is limited by the small sample size of the treatment arm, with analysis of trends/relationships between intratumoral evolocumab and HLA-A, B, -C and ApoE limited to just 4 cases. This study was primarily a biologically driven mechanistic study for establishing the PK and PD characteristics of a single pre-operative dose of evolocumab. Although there was potential for therapeutic benefit with increased $CD8^+$ infiltration into tumors, the treatment course of just one dose of evolocumab likely reduced patient accrual and precluded drawing substantive clinical conclusions. Accrual in future tissue-based studies will most likely be enhanced by offering sustained therapeutic intervention after tissue acquisition and analyses. However, Window of Opportunity studies afford us the ability to quickly assess the impact of treatment. Given the suggestion of increased biological effect with greater PCSK9i in tumor, but uptake ratios for both contrast and non-contrast enhancing disease in keeping with other mAbs, we can rationalize early modification of our treatment approach. Future approaches may include combination alongside modalities that increase uptake/PCSK9i in the brain such as low-intensity focused ultrasound (LIFU), which can transiently open the BBB/BTB to larger constructs (*40, 41*). Transient BBB/BTB opening may also facilitate greater uptake of ICB therapies which could be administered simultaneously alongside LIFU and evolocumab as part of a multi-pronged approach. Alternate strategies to aid BBB/BTB penetration of PCSK9i could also consider lipid nanoparticle encapsulation of PCSK9 siRNA (*42*).

We also had to consider how to optimally use biospecimens. In this study, patients underwent clinically indicated resection or biopsy. Appropriately, tissue allocation was first prioritized for clinical/diagnostic purposes, with excess being made available for research. However, this posed a particular challenge in needle biopsy cases where tissue cores are just ~10-15mg in size. Nevertheless, for cases where excess tissue was available, LC/MS-MS drug quantitation, tumor proteome analysis and IHC/IF staining were feasible, even with a handful of biopsy cores. However, limited sample volumes limited our capability to perform more detailed pharmacokinetic analyses, such as evaluating the ratio of free to unbound drug. Appropriate selection of PK/PD analysis techniques that can utilize predicted quantities of tissue requires careful consideration prior to study initiation. Future tissue-based trials evaluating drug PK will also need to consider the potential of peripheral blood contamination in tissue samples. This is particularly problematic when

attempting to detect low levels of drug in tissue (as will likely be the case in SWOOPP studies conducted in the CNS). Processes to minimize cross contamination can range from simple (e.g., rinsing tissue with saline to remove excess blood) to complex (normalization to quantitated hemoglobin protein levels in tissue and blood), but there is little validation regarding the relative efficacy of these. Ultimately, standardized processes to assess drug quantitation (PK) and biological effect (PD) are required. This will require harmonization of approaches to remove confounding drug signal from peripheral blood and agreed LC-MS/MS protocols for quantitation of protein levels in tissue.

Although this study included a control group using samples from non-treated patients, our primary objective was detection of drug in tumor (PK). In this setting, presence of drug is a binary question (yes/no) and tissue from untreated patients can be used as an appropriate control. For assessment of biological effect, the tumoral immune landscape can be highly variable between patients (*43*). Contemporaneous controls from a separate non-treated patient group are therefore suboptimal as a comparator for immune landscape changes, particularly when a mixture of glioma pathologies is eligible for inclusion (as was the case here to facilitate recruitment). Alternative suggested approaches include using tissue from the same patient, taken at the time of initial resection. However, tumors can evolve following treatment and the immune landscape of a tumor at recurrence can differ greatly from that at initial presentation (*44*). While there are increasing calls for greater longitudinal tissue sampling from patients with glioblastoma, including pre-treatment biopsies in tissue-based trials, this is not yet standard practice (*45*). In the interim, newer tissue-based trial designs (NCT05634707) have included optional pre-treatment biopsies for patients in which true recurrence is uncertain and a biopsy would be clinically helpful (e.g., if querying pseudoprogression (*46*)). When available, these pre-treatment biopsies are vital as internal controls to validate baseline characteristics in other control group types (contemporaneous, historical, case-matched controls etc.). Our framework for rationalizing control groups in tissue-based studies, along with key considerations when selecting samples is shown in **Fig. 7.**

In conclusion, pre-operative high-dose evolocumab in patients undergoing resection or biopsy for glioma appears to be well tolerated. However, uptake of evolocumab across the BBB/BTB is in keeping with other antibody therapies, with highest uptake observed in cases with the greatest degree of contrast-enhancement (average tumor:blood ratio of 0.0332 in contrast-enhancing cases vs 0.0112 in non-contrast-enhancing cases). Despite this, we find suggestions of mechanistic effect of PCSK9i in the context of high-grade glioma. Increased MHC-I expression and $CD8^+$ T cell infiltration was observed in grade IV gliomas with higher evolocumab detection, while ApoE levels declined in a linear fashion, indicative of a dose-dependent biological effect. Future work will explore combination strategies that can enhance evolocumab uptake into high-grade gliomas, such as low-intensity focused ultrasound.

## MATERIALS AND METHODS

### Study oversight and design

PesKE is a non-randomized, open-label, single-center surgical window of opportunity study that is being conducted to assess if Evolocumab, a clinically approved drug for hypercholesteremia, can cross the blood brain barrier and accumulate within the brain tumor of patients with glioma or glioblastoma. Study participants included newly diagnosed or recurrent patients who are due to undergo resection or biopsy of their tumor. Up to 10 patients were to be enrolled in the treatment arm of this study, while up to 20 patients served as controls.

The study received approval by the institutional review board at the Duke Cancer Institute (DCI, Duke IRB# Pro000108375). Study monitoring was performed both internally by the Principal Investigator (PI) and institutionally by the DCI. Audits of compliance with

the protocol and principles of Good Clinical Practice were routinely performed by the Duke Office of Audit, Risk and Compliance (OARC). Data and Safety Monitoring were performed in accordance with the DCI Data and Safety Monitoring Plan.
This study recruited adult patients (≥ 18 years old) with newly diagnosed or recurrent glioma and who had a clinical indication for either gross macroscopic resection, debulking, or biopsy of their disease. Participants were enrolled if pre-operative imaging indicated a sufficient tumor size that would allow for collection of specimens for the required analyses. Tissue for research purposes was only taken after sufficient tissue for clinical diagnostic purposes was collected. Once enrolled, participants on the treatment arm received 420 mg of Evolocumab (administered subcutaneously) 4-14 days prior to their surgical procedure. Participants were assigned to the treatment arm if it was logistically feasible for them to receive subcutaneous evolocumab prior to their planned procedure (i.e., patients could attend for pre-operative administration of drug within the study's timeframe of 4-14 days prior to procedure).

Participants assigned to the control arm received no treatment prior to surgery. All participants enrolled in the study were assigned to have an intra-operative blood draw at the time of tissue collection. Treatment patients also underwent a blood draw prior to evolocumab administration. Participants on the treatment arm were then followed up for two weeks following surgery or biopsy and monitored for adverse events as well as routine post-operative assessments of physical and neurological status as well as standard laboratory evaluations. An overview of the study design is shown in **Fig. S2.**, and the full study protocol is available at clinicaltrials.gov (NCT04937413).

**Tissue handling**

Following surgery, samples were received in the surgical pathology laboratory and examined by the diagnostic staff. Areas suspicious for tumor were examined by frozen section by a neuropathologist. Once the diagnosis of tumor was established, tissue in excess of that required for an adequate and accurate diagnosis were collected and processed by members of the technical staff of the Duke Brain Tumor Biorepository (BTBR), a College of American Pathologists certified biorepository. Tissues were snap-frozen in liquid nitrogen either plain or embedded into Optimal Cutting Temperature (OCT) compound. If tissue samples were excessively bloody, they were rinsed with saline prior to freezing. Time as well as sample dimensions and weights were recorded at the point of freezing. At the time of surgery, whole blood was collected in tubes containing Ethylenediaminetetraacetic acid (EDTA) and placed on dry ice for transfer to storage. After freezing, samples were stored in liquid nitrogen and transferred to -80 °C prior to proteomic analysis. Sample collection details were maintained in the BTBR's Nautilus laboratory information management system (LIS), with clinical details maintained in REDCAP. After samples were checked into the BTBR LIS, they were then distributed to research teams for downstream analysis.

**Immunohistochemistry & Immunofluorescence**

IHC and IF sectioning, staining, and imaging were performed at an external vendor (HistoWiz Inc). Staining was performed via a Leica bond automated staining platform, Akoya imager, and a proprietary processing, embedding, and grossing workflow. IHC stains were performed for $CD45^+$ (1:100, Abcam #ab40763) and $CD8^+$ (1:200, Leica #NCL-L-CD8-4B11). Triplex IF co-stained for Wheat Germ Agglutinin (WGA, 1:100, Invitrogen #W11261), MHC-I (1:3000, Cell Signaling #88274) and Glial Fibrillary Acidic Protein (GFAP, 1:6000, Novus #NB300-141) with DAPI counterstain.

**Mass Spectroscopy**

For targeted assay development, 30 µg of neat evolocumab, or 30 or 100 pmol evolocumab in 20 µL of pooled human plasma (Golden West Diagnostics) were processed as previously described (*27*). Briefly, samples were diluted to 200 µL with 5% deoxycholate and 10

mM dithiothreitol (DTT) followed by heating at 80 °C for 20 min using a Thermomixer (Eppendorf). After cooling, alkylation was performed with 25 mM iodoacetamide in the dark for 30 min followed by the addition of 100 µg of TPCK-trypsin (Worthington) and incubation at 37 °C for 2 h. After quenching with 1.5% trifluoroacetic acid and filtering, digests were analyzed by a 20 min microflow LC-MS/MS using a Waters ACQUITY UPLC (1 x 100 mm or 1 x 150 mm ACQUITY Premier CSH column; direct injection; 100 µL/min flow rate; 3-28% MeCN-0.1% formic acid) interfaced to a Thermo Exploris 480. Neat Evo was analyzed by data-dependent acquisition, and database searching was performed with Skyline (*47*) using the MS Amanda search engine with Percolator post-search validation (*48, 49*). Peptide uniqueness was predicted using NCBI BLASTp and Nextprot peptide uniqueness checker (*50*). Candidate proteotypic peptides were analyzed in the evolocumab-spiked plasma using parallel reaction monitoring as previously described. Data were analyzed in Skyline and have been uploaded to the ProteomeXchange consortium (details in data and materials availability sub-section).

For targeted quantification of evolocumab in whole blood, 20 µL of EDTA-blood was spiked with 2 pmol of JPT SpikeTides TQL peptides with the sequences ASGYTLTSYGISWVR, GTMTTDPSTSTAYMELR and GYGMDVWGQGTTVTVSSASTK (and 10 pmol of evolocumab in positive control samples) followed by deoxycholate-assisted trypsin digestion and microflow LC-MS/MS with solvent divert as described previously (*27*). Briefly, deoxycholate-assisted trypsin digestion was used above except that 500 µg of TPCK-trypsin was used and reactions were quenched with 2% TFA. An external calibration curve was generated using evolocumab in whole blood from a control subject, and quantification to standard curve was performed using Skyline. Blood levels (normalized to volume) were further normalized to microgram protein (fmol/µg) based on an estimated protein concentration in blood of 250 µg/µL.

Fresh frozen tissue either directly frozen or embedded in OCT were analyzed using targeted and non-targeted proteomics. Briefly, tissue was rinsed free with cold phosphate-buffered saline and homogenized by sonication or bead beating in a 10:1 volume per tissue weight of 5% (w/v) sodium dodecyl sulfate in 50 mM triethylammonium bicarbonate. Based on detergent-compatible Bradford assay, 20 µg of each sample was reduced and alkylated and digested with 2 or 10 µg Sequencing Grade Modified Trypsin (Promega) using an S-trap micro device (Protifi) and 47 °C for 1 h. 200 fmol of SpikeTides TQL peptides were added to the S-trap along with trypsin. After elution, peptides were lyophilized, reconstituted in 0.2 % formic acid, and a study pool QC (SPQC) sample was made by mixing equal amounts of all samples. Approximately 1 µg of each sample, along with replicates of a study pool QC (SPQC), were loaded onto Evotip Pure tips. Targeted proteomic analysis used an Evosep One LC interfaced to a Thermo Exploris 480 and analyzed using a 100 sample-per-day (100SPD) LC method and PRM as described above. During method development, 100 µg of select samples were digested with 10 µg trypsin, and 30 µg of digested were analyzed by microflow LC-MS/MS as with the whole blood. Data was analyzed in Skyline and normalized to stable isotope-labeled internal standard (at 10 fmol/µg) to derive femtomol per microgram values of evolocumab in tumor.

Non-targeted proteomics used an Evosep One LC interfaced to a Thermo Orbitrap Astral using a 60 sample-per-day (60SPD) LC method and data-independent acquisition (DIA) in the Astral analyzer (*51, 52*). MS/MS used 150 x 4 m/z windows from 380-980 m/z, and automatic gain control target of 500%, 6 ms ion transfer time and normalized collision energy of 28. Data was analyzed with DIA-NN 1.8.2 beta 27 in library-free mode (*53*). Raw data was converted to .dia before processing. Default settings were used with trypsin specificity and up to 2 missed cleavage, and N-terminal acetylation as a variable modification, Identification and quantification used a 1% precursor and protein group false discovery rate. Data was further filtered to include protein groups with no missing data and %coefficient of variation <50 across four analyses of a QC pool.

**Graphical illustrations**

Graphical illustrations in **Fig. 7** and **Fig. S1** were created with BioRender.com and exported using a paid license.

**Statistics**

Experimental results are presented as mean ± SD unless otherwise specified. Statistical tests for all studies were completed using GraphPad v.8.4.3 (Prism). Asterisks were appended to graphs to represent the significance level of any difference (*$p \leq 0.05$, **$p \leq 0.01$, ***$p \leq 0.001$, ****$p \leq 0.0001$, $p > 0.05$ not significant). Correlation analyses were performed using the Pearson correlation coefficient. For comparisons in a single graph, two-tailed Mann-Whitney U tests were used.

# References and Notes:


1. A. M. Cornel, I. L. Mimpen, S. Nierkens, MHC class I downregulation in cancer: underlying mechanisms and potential targets for cancer immunotherapy. *Cancers* **12**, 1760 (2020).
2. M. D. Farwell *et al.*, CD8-Targeted PET Imaging of Tumor-Infiltrating T Cells in Patients with Cancer: A Phase I First-in-Humans Study of (89)Zr-Df-IAB22M2C, a Radiolabeled Anti-CD8 Minibody. *J Nucl Med* **63**, 720-726 (2022).
3. M. Mina *et al.*, Tumor-infiltrating T lymphocytes improve clinical outcome of therapy-resistant neuroblastoma. *OncoImmunology* **4**, e1019981 (2015).
4. R. Squire, C. L. Fowler, S. P. Brooks, G. A. Rich, D. R. Cooney, The relationship of class I MHC antigen expression to stage IV-S disease and survival in neuroblastoma. *Journal of pediatric surgery* **25**, 381-386 (1990).
5. E. C. Lerner *et al.*, CD8+ T cells maintain killing of MHC-I-negative tumor cells through the NKG2D–NKG2DL axis. *Nature Cancer* **4**, 1258-1272 (2023).
6. B. J. Morrison, J. C. Steel, J. C. Morris, Reduction of MHC-I expression limits T-lymphocyte-mediated killing of Cancer-initiating cells. *BMC cancer* **18**, 1-10 (2018).
7. F. Garrido, N. Aptsiauri, E. M. Doorduijn, A. M. G. Lora, T. Van Hall, The urgent need to recover MHC class I in cancers for effective immunotherapy. *Current opinion in immunology* **39**, 44-51 (2016).
8. N. Naslavsky, R. Weigert, J. G. Donaldson, Characterization of a nonclathrin endocytic pathway: membrane cargo and lipid requirements. *Mol Biol Cell* **15**, 3542-3552 (2004).
9. X. Liu *et al.*, The immune functions of PCSK9: Local and systemic perspectives. *J Cell Physiol* **234**, 19180-19188 (2019).
10. S. Poirier *et al.*, The proprotein convertase PCSK9 induces the degradation of low density lipoprotein receptor (LDLR) and its closest family members VLDLR and ApoER2. *J Biol Chem* **283**, 2363-2372 (2008).
11. A. Demers *et al.*, PCSK9 Induces CD36 Degradation and Affects Long-Chain Fatty Acid Uptake and Triglyceride Metabolism in Adipocytes and in Mouse Liver. *Arterioscler Thromb Vasc Biol* **35**, 2517-2525 (2015).
12. X. Liu *et al.*, Inhibition of PCSK9 potentiates immune checkpoint therapy for cancer. *Nature* **588**, 693-698 (2020).
13. M. Uhlén *et al.*, Tissue-based map of the human proteome. *Science* **347**, 1260419 (2015).
14. K. Singh *et al.*, Designing Clinical Trials for Combination Immunotherapy: A Framework for Glioblastoma. *Clinical cancer research : an official journal of the American Association for Cancer Research* **28**, 585-593 (2022).
15. M. S. Sabatine *et al.*, Efficacy and Safety of Evolocumab in Reducing Lipids and Cardiovascular Events. *New England Journal of Medicine* **372**, 1500-1509 (2015).
16. M. S. Sabatine, PCSK9 inhibitors: clinical evidence and implementation. *Nature Reviews Cardiology* **16**, 155-165 (2019).
17. G. G. Schwartz *et al.*, Alirocumab and Cardiovascular Outcomes after Acute Coronary Syndrome. *New England Journal of Medicine* **379**, 2097-2107 (2018).
18. N. G. Seidah, A. Prat, The biology and therapeutic targeting of the proprotein convertases. *Nat Rev Drug Discov* **11**, 367-383 (2012).
19. K. Fitzgerald *et al.*, A Highly Durable RNAi Therapeutic Inhibitor of PCSK9. *The New England journal of medicine* **376**, 41-51 (2017).
20. J. P. Gibbs *et al.*, Impact of Target-Mediated Elimination on the Dose and Regimen of Evolocumab, a Human Monoclonal Antibody Against Proprotein Convertase Subtilisin/Kexin Type 9 (PCSK9). *The Journal of Clinical Pharmacology* **57**, 616-626 (2017).
21. W. M. Pardridge, Blood-Brain Barrier and Delivery of Protein and Gene Therapeutics to Brain. *Frontiers in Aging Neuroscience* **11**, (2020).
22. B. M. Marin *et al.*, Heterogeneous delivery across the blood-brain barrier limits the efficacy of an EGFR-targeting antibody drug conjugate in glioblastoma. *Neuro-oncology* **23**, 2042-2053 (2021).
23. J. N. Sarkaria *et al.*, Is the blood-brain barrier really disrupted in all glioblastomas? A critical assessment of existing clinical data. *Neuro-oncology* **20**, 184-191 (2018).
24. J. Portnow *et al.*, Systemic Anti-PD-1 Immunotherapy Results in PD-1 Blockade on T Cells in the Cerebrospinal Fluid. *JAMA oncology* **6**, 1947-1951 (2020).
25. K. F. Schulz, D. G. Altman, D. Moher, CONSORT 2010 statement: updated guidelines for reporting parallel group randomised trials. *Bmj* **340**, c332 (2010).
26. M. Schaeffer *et al.*, The neXtProt peptide uniqueness checker: a tool for the proteomics community. *Bioinformatics* **33**, 3471-3472 (2017).
27. T. H. Schaller *et al.*, Pharmacokinetic Analysis of a Novel Human EGFRvIII:CD3 Bispecific Antibody in Plasma and Whole Blood Using a High-Resolution Targeted Mass Spectrometry Approach. *J Proteome Res* **18**, 3032-3041 (2019).
28. T. Y. Jung *et al.*, Immunological characterization of glioblastoma cells for immunotherapy. *Anticancer research* **33**, 2525-2533 (2013).
29. R. W. Mahley, Central Nervous System Lipoproteins. *Arteriosclerosis, Thrombosis, and Vascular Biology* **36**, 1305-1315 (2016).

30. D. A. Reardon *et al.*, Effect of Nivolumab vs Bevacizumab in Patients With Recurrent Glioblastoma: The CheckMate 143 Phase 3 Randomized Clinical Trial. *JAMA Oncology* **6**, 1003-1010 (2020).
31. K. Maddison *et al.*, Low tumour-infiltrating lymphocyte density in primary and recurrent glioblastoma. *Oncotarget* **12**, 2177-2187 (2021).
32. M. H. Robinson *et al.*, Subtype and grade-dependent spatial heterogeneity of T-cell infiltration in pediatric glioma. *Journal for ImmunoTherapy of Cancer* **8**, e001066 (2020).
33. L. Ren *et al.*, Apolipoproteins and cancer. *Cancer Med* **8**, 7032-7043 (2019).
34. G. Miao *et al.*, From degenerative disease to malignant tumors: Insight to the function of ApoE. *Biomedicine & Pharmacotherapy* **158**, 114127 (2023).
35. M. F. Lanfranco, J. Sepulveda, G. Kopetsky, G. W. Rebeck, Expression and secretion of apoE isoforms in astrocytes and microglia during inflammation. *Glia* **69**, 1478-1493 (2021).
36. H. Zhang, L.-M. Wu, J. Wu, Cross-talk between apolipoprotein E and cytokines. *Mediators of inflammation* **2011**, (2011).
37. D. Baitsch *et al.*, Apolipoprotein E induces antiinflammatory phenotype in macrophages. *Arteriosclerosis, thrombosis, and vascular biology* **31**, 1160-1168 (2011).
38. F. Khan *et al.*, Macrophages and microglia in glioblastoma: heterogeneity, plasticity, and therapy. *The Journal of clinical investigation* **133**, (2023).
39. F. Liao *et al.*, Anti-ApoE antibody given after plaque onset decreases Aβ accumulation and improves brain function in a mouse model of Aβ amyloidosis. *Journal of Neuroscience* **34**, 7281-7292 (2014).
40. Y. Huang *et al.*, Cavitation Feedback Control of Focused Ultrasound Blood-Brain Barrier Opening for Drug Delivery in Patients with Parkinson's Disease. *Pharmaceutics* **14**, (2022).
41. P. Y. Chen *et al.*, Focused ultrasound-induced blood-brain barrier opening to enhance interleukin-12 delivery for brain tumor immunotherapy: a preclinical feasibility study. *J Transl Med* **13**, 93 (2015).
42. T. Kalita, S. A. Dezfouli, L. M. Pandey, H. Uludag, siRNA Functionalized Lipid Nanoparticles (LNPs) in Management of Diseases. *Pharmaceutics* **14**, (2022).
43. E. Karimi *et al.*, Single-cell spatial immune landscapes of primary and metastatic brain tumours. *Nature* **614**, 555-563 (2023).
44. A. T. Yeo *et al.*, Single-cell RNA sequencing reveals evolution of immune landscape during glioblastoma progression. *Nature Immunology* **23**, 971-984 (2022).
45. K. Singh *et al.*, Correcting the drug development paradigm for glioblastoma requires serial tissue sampling. *Nat Med* **29**, 2402-2405 (2023).
46. S. C. Thust, M. J. van den Bent, M. Smits, Pseudoprogression of brain tumors. *J Magn Reson Imaging* **48**, 571-589 (2018).
47. L. K. Pino *et al.*, The Skyline ecosystem: Informatics for quantitative mass spectrometry proteomics. *Mass Spectrom Rev* **39**, 229-244 (2020).
48. V. Dorfer *et al.*, MS Amanda, a universal identification algorithm optimized for high accuracy tandem mass spectra. *J Proteome Res* **13**, 3679-3684 (2014).
49. L. Käll, J. D. Canterbury, J. Weston, W. S. Noble, M. J. MacCoss, Semi-supervised learning for peptide identification from shotgun proteomics datasets. *Nat Methods* **4**, 923-925 (2007).
50. M. Zahn-Zabal *et al.*, The neXtProt knowledgebase in 2020: data, tools and usability improvements. *Nucleic Acids Res* **48**, D328-d334 (2020).
51. U. H. Guzman *et al.*, Ultra-fast label-free quantification and comprehensive proteome coverage with narrow-window data-independent acquisition. *Nat Biotechnol*, (2024).
52. L. R. Heil *et al.*, Evaluating the Performance of the Astral Mass Analyzer for Quantitative Proteomics Using Data-Independent Acquisition. *J Proteome Res* **22**, 3290-3300 (2023).
53. V. Demichev, C. B. Messner, S. I. Vernardis, K. S. Lilley, M. Ralser, DIA-NN: neural networks and interference correction enable deep proteome coverage in high throughput. *Nat Methods* **17**, 41-44 (2020).

# Acknowledgements:

**General**

We are grateful to all patients and their caregivers who enrolled in this study. We are also grateful to the Knox Martin Foundation and the Langford Cregger Foundation for their philanthropic support. We are also grateful to the team at the Duke Brain Tumor Biorepository for their assistance and co-ordination in tissue management and acquisition.

**Funding**

Knox Martin Foundation, Philanthropic Grant (MK)

Langford Cregger Foundation, Philanthropic Grant (MK)

**Author contributions**

Conceptualization: KS, MK

Methodology: KS, MWF, MJV, MK

Investigation: KS, MWF, MJV, ELT, KMH, COR, EEB, DMA, AD, HSF, MOJ, AF, SK, JHS, APP, CYL

Pathology: GYL, REM

Neuroradiology: EC

Writing – original draft: KS, MWF, PEF, MK

Writing – review & editing: KS, MWF, MJV, ELT, KMH, COR, EEB, DMA, AD, HSF, MOJ, AF, SK, JHS, APP, CYL, PEF, MK

Statistical analysis: KS, EDB, JEH

Supervision: PEF, MK

**Competing Interests**

KS, MWF, MJV, KMH, COR, EEB, KEB, ELT, DMA, AD, HSF, MOJ, AF, SK, EDB, JEH, REM, EC, GAG, CYL declare that they have no competing interests. JHS reports an equity interest in Istari Oncology, which has licensed intellectual property from Duke related to the use of poliovirus and D2C7 in the treatment of glioblastoma. JHS is an inventor on patents related to Brain Bi-specific T cell Engagers (BRiTE), PEP-CMV DC vaccine with tetanus, as well as poliovirus vaccine and D2C7 in the treatment of glioblastoma. GYL reports consulting fees from Servier Pharmaceuticals. GYL is a consultant for and has equity in SNPsnipe, Inc. APP is a consultant for Sygnomics, Syapse, and Servier Pharmaceuticals, and has an equity in Sygnomics. PEF reports support as an Akash fellow of the CRI Lloyd J. Old STAR award program and has received consulting fees and grant funding from Monteris Medical outside the submitted work. MK reports grants or contracts from BMS, AbbVie, BioNTech, CNS Pharmaceuticals, Daiichi Sankyo Inc., Immorna Therapeutics, Immvira Therapeutics, JAX lab for genomic research, and Personalis, Inc.; received consulting fees from AnHeart Therapeutics, Berg Pharma, George Clinical, Manarini Stemline, and Servier; received honoraria from GSK; and is on a data safety monitoring board for BPG Bio.

**Data and materials availability**

Targeted proteomic data have been deposited to the ProteomeXchange Consortium (PXD053215) via the Panorama Public repository (https://panoramaweb.org/ccb1LM.url). All demographic, AE, flow cytometry and IHC/IF data is available in the main text.

# Supplementary Materials:

**List: Fig. S1. to S2.** Mechanism of PCSK9i for increasing surface MHC-I and study schema. No SM specific references.

## Fig. 1. Relative plasma concentrations of PCSK9 in blood from patients with different cancer types

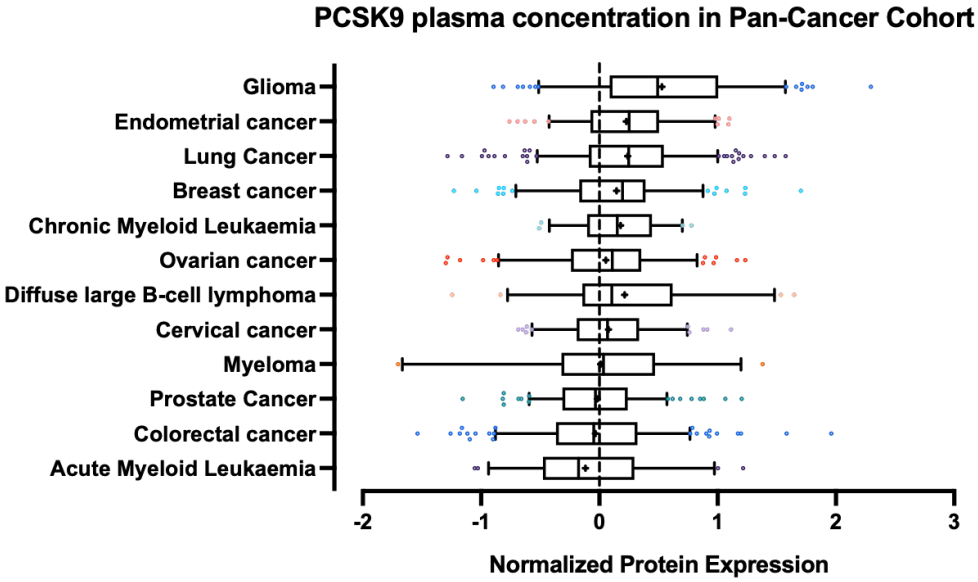


| Pathology | N | Median Change (95% CI) |
|---|---|---|
| Glioma | 145 | 0.493 (0.378 to 0.663) |
| Endometrial | 101 | 0.252 (0.132 to 0.328) |
| Lung | 268 | 0.248 (0.155 to 0.317) |
| Breast | 152 | 0.196 (0.072 to 0.264) |
| CML | 48 | 0.151 (0 to 0.375) |
| Ovarian | 134 | 0.109 (0.014 to 0.192) |
| DLBCL | 55 | 0.106 (-0.006 to 0.314) |
| Cervical | 102 | 0.069 (-0.007 to 0.159) |
| Myeloma | 38 | 0.036 (-0.19 to 0.296) |
| Prostate | 162 | -0.033 (-0.111 to 0.07) |
| Colorectal | 221 | -0.048 (-0.126 to 0.061) |
| AML | 50 | -0.177 (-0.395 to 0.063) |

**Fig. 1. Relative plasma concentrations of PCSK9 in blood from patients with different cancer types**

Box and whisker representations of circulating concentrations of PCSK9 protein in plasma across multiple cancer types. Circulating plasma PCSK9 protein levels are the most upregulated in glioma compared to the average concentration from samples across multiple. Assessed by proximity extension assay (PEA). Whiskers represent 5-95% range with outliers shown. Mean shown as +. Data from proteinatlas.org (https://www.proteinatlas.org/ENSG00000169174-PCSK9/disease).

**Fig. 2. CONSORT flow diagram of enrolled participants**

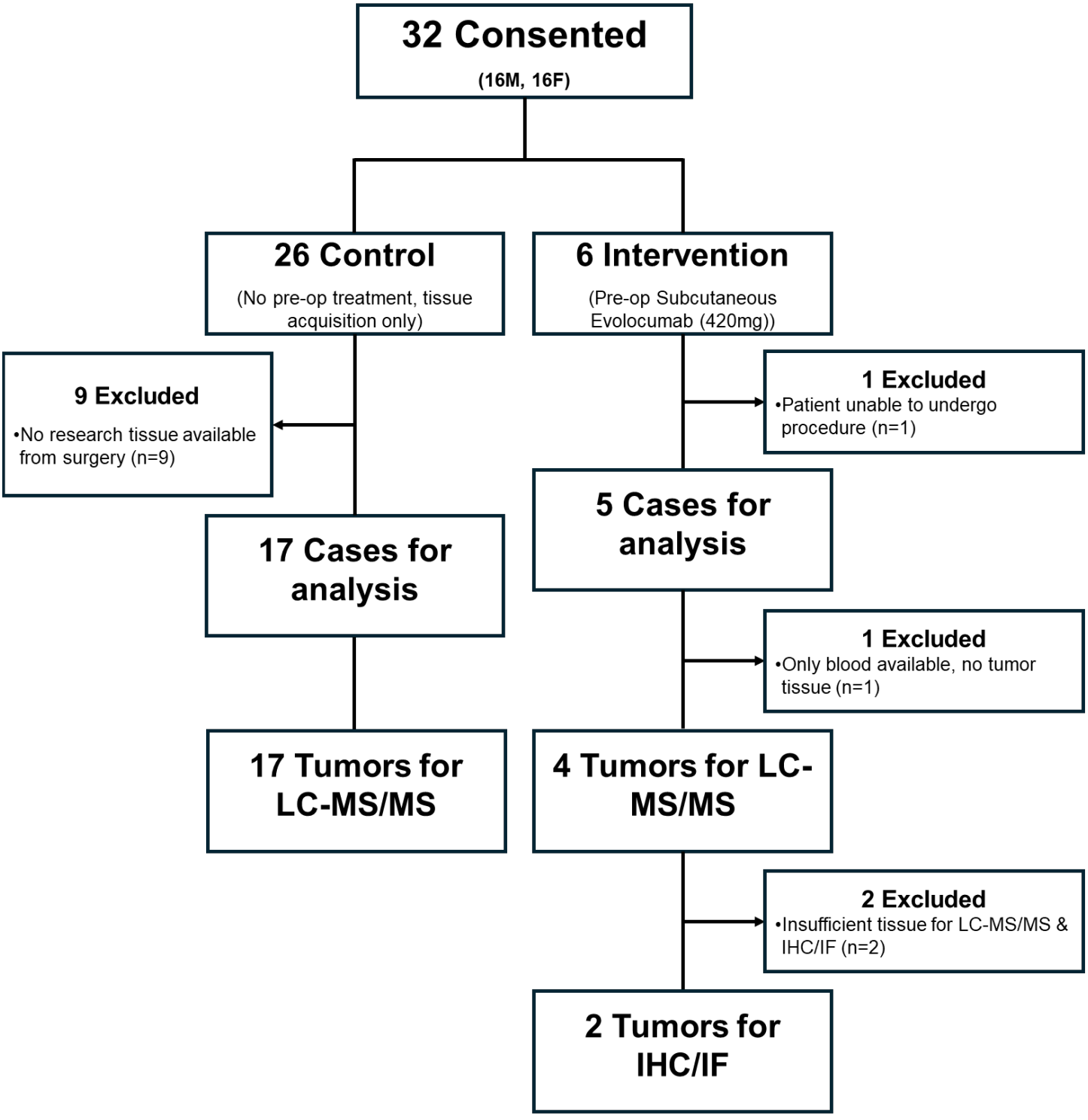


*Tissue only collected for research purposes if excess available beyond that required for clinical pathology.

**Fig. 3. Evolocumab is detectable at higher levels in contrast-enhancing tumors, but has low BBB/BTB penetrance overall**

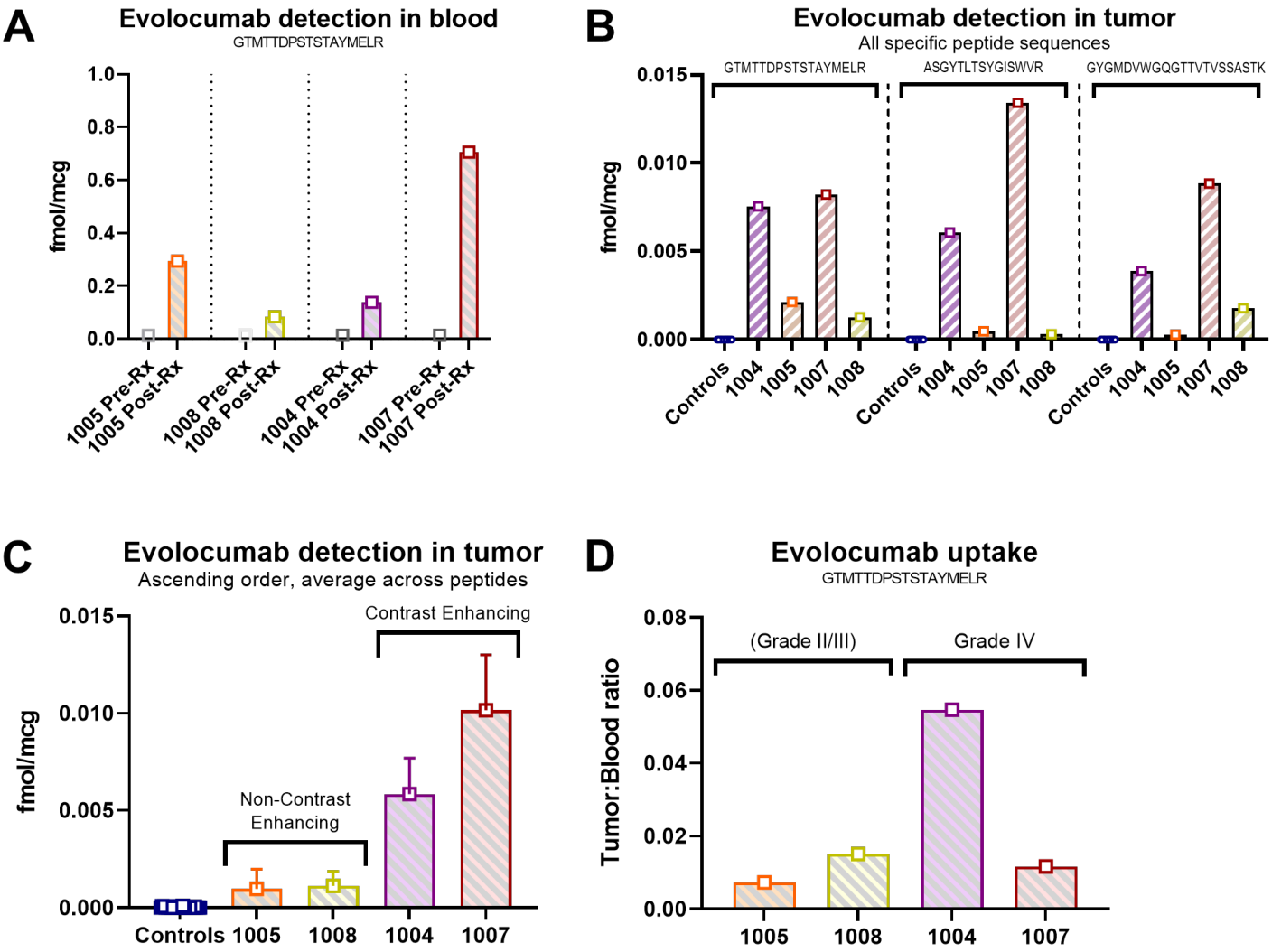

**Fig. 3. Evolocumab is detectable at higher levels in contrast-enhancing tumors, but has low BBB/BTB penetrance overall**

(A) Evolocumab levels in peripheral blood (1005: 0.2940 fmol/mcg, 1008: 0.0836 fmol/mcg, 1004: 0.1383 fmol/mcg, 1007: 0.7052 fmol/mcg). No evolocumab was detected in pre-treatment blood samples. Detection via most specific evolocumab detection peptide (GTMTTDPSTSTAYMELR) shown in analysis.

(B) Evaluation of evolocumab in tumor samples using the three specific peptide sequences (ASGYTLTSYGISWVR, GTMTTDPSTSTAYMELR and GYGMDVWGQGTTVTVSSASTK) that are not part of the human proteome but specifically identify drug with minimal background. Detection is normalized to stable internally labelled (SIL) peptide controls. Similar patterns in evolocumab levels are observed across all 4 treatment cases, with minimal background signal seen in control cases.

(C) Evolocumab levels in tumor were higher in cases 1004 and 1007 (0.005838 fmol/mcg and 0.01016 fmol/mcg respectively), whereas detection was lower in cases 1005 and 1008 (0.000964 fmol/mcg and 0.001118 fmol/mcg respectively). Average across individual detection peptides for each case outlined in (A) shown.

(D) Tumor:blood ratios for grade II/III and grade IV lesions. Greater uptake was observed in contrast-enhancing tumors with an average tumor:blood ratio of 0.0332 (SD±0.0215), while non-contrast-enhancing cases had an average tumor:blood ratio of 0.0112 (SD±0.0039). The greatest uptake ratio was observed in the case with the highest degree of contrast-enhancement on MRI (ID: 1004, tumor:blood ratio of 0.0547, MRI shown in **Fig. 4C**). Detection via most specific evolocumab detection peptide (GTMTTDPSTSTAYMELR) shown in analysis.

Data presented as mean ± SD unless otherwise specified.

**Fig. 4. MRI sequences of tumors with lower and higher evolocumab (EVO) uptake**

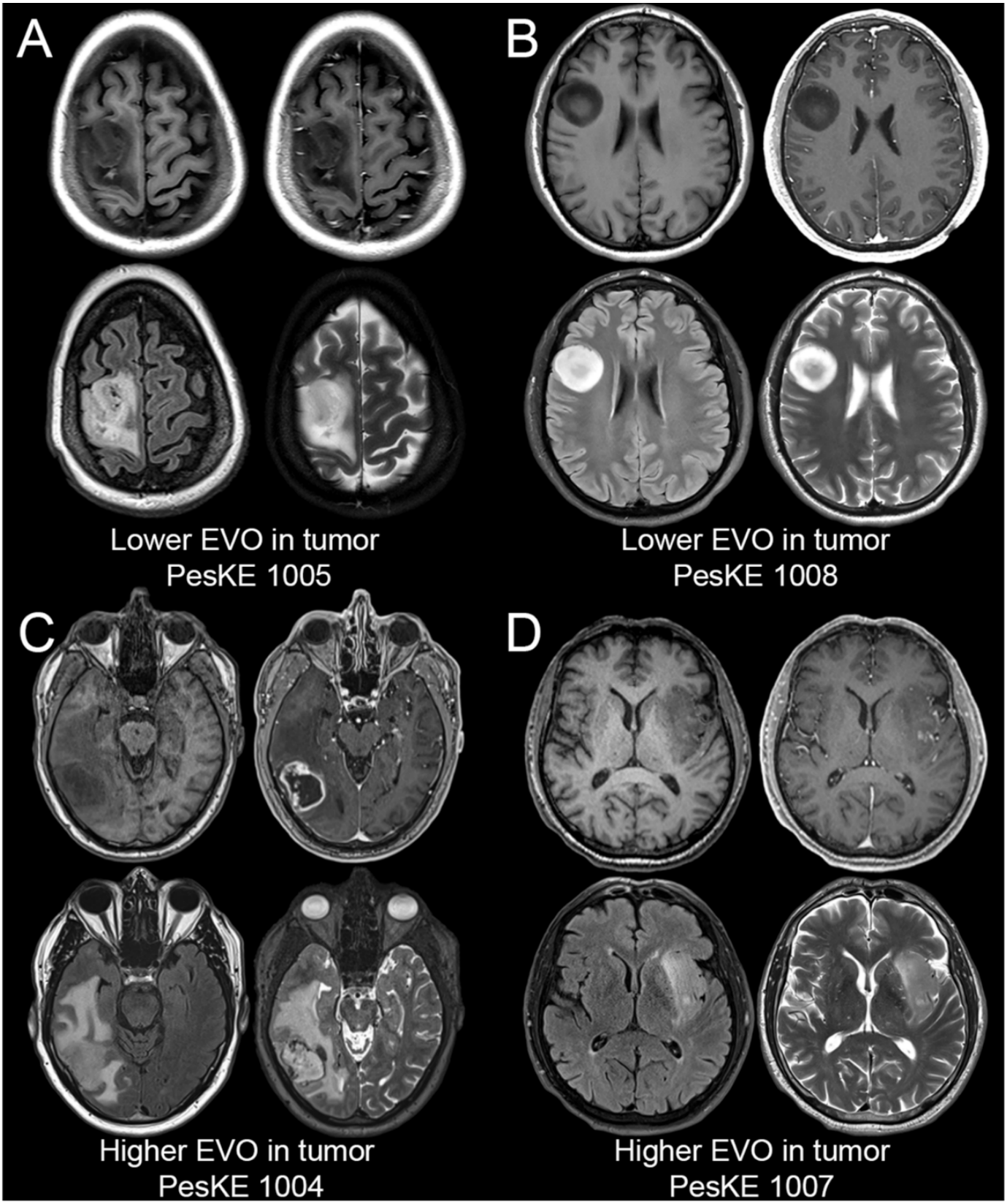


*Representative pre-operative brain MRI images of intervention tumors. For each panel A-D, axial images through the tumor are shown from four standard anatomic image series (clockwise from left: T1-weighted pre-contrast, T1-weighted post-contrast, T2-weighted, and T2-weighted FLAIR).*

**Fig. 4. MRI sequences of tumors with lower and higher evolocumab (EVO) uptake**

(A & B) Evaluation of pre-operative MR imaging from cases 1005 (grade III Oligodendroglioma) and 1008 (grade II Astrocytoma) with lower evolocumab uptake reveals non-contrast-enhancing lesions on T1 post sequences (quadrant top-right).

(C & D) Conversely, evaluation of pre-operative MR imaging from cases 1004 and 1007 (both grade IV glioblastomas) with higher evolocumab uptake reveals evidence of contrast-enhancement on T1 post sequences (quadrant top-right).

Representative pre-operative brain MRI images of analyzed tumors. For each panel A-D, axial images through the tumor are shown from four standard anatomic image series (clockwise from left: T1-weighted pre-contrast, T1-weighted post-contrast, T2-weighted, and T2-weighted FLAIR).

**Fig. 5. Glioma tissue with higher evolocumab uptake exhibits increased HLA-A and -B and decreased Apolipoprotein E in the tumor proteome**

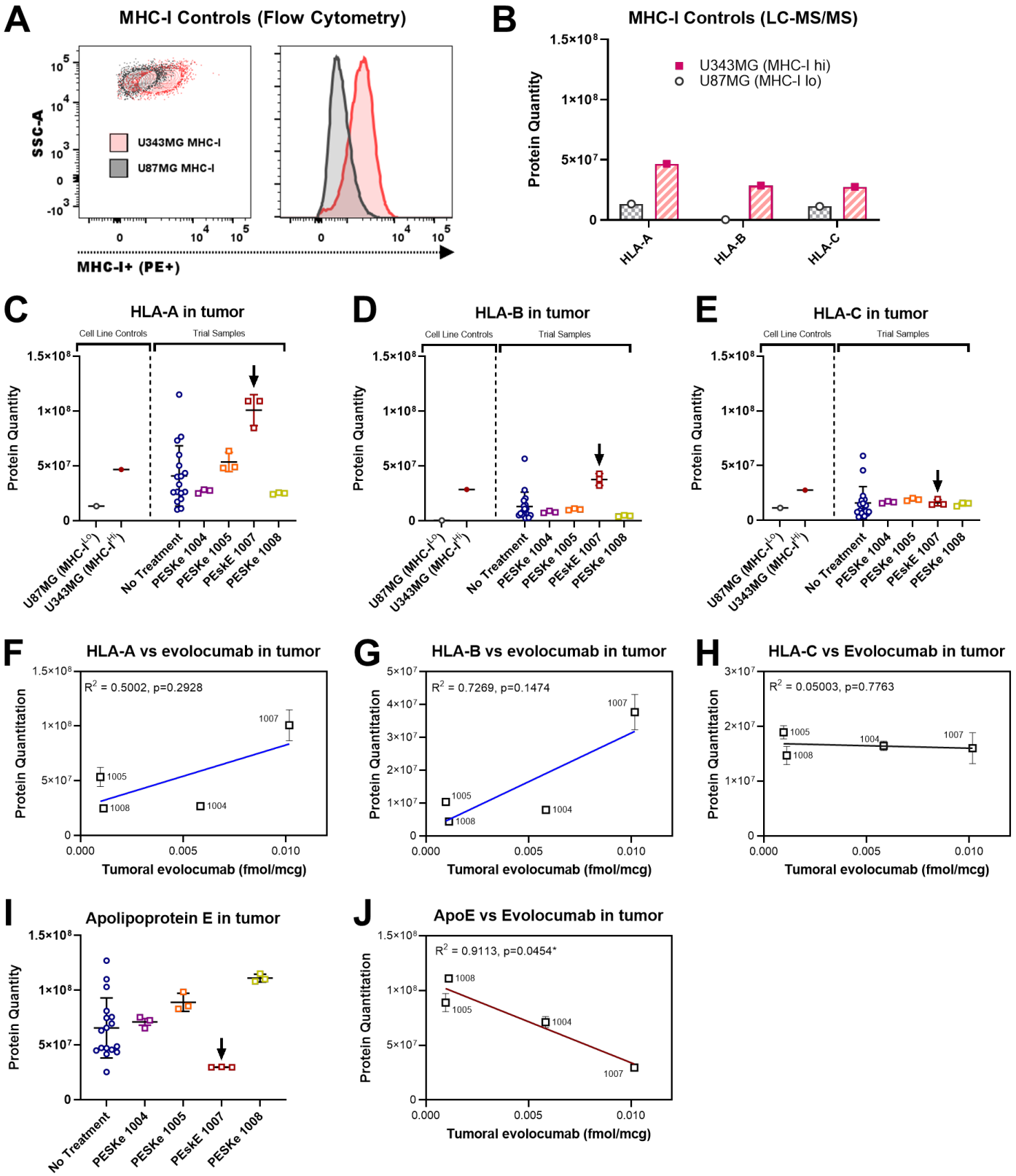

**Fig. 5. Glioma tissue with higher evolocumab uptake exhibits increased HLA-A and -B and decreased Apolipoprotein E in the tumor proteome**

(A) Flow cytometric analysis of immortalized human glioma lines thought to express higher (U343MG, red) or lower (U87MG, black) levels of MHC-I. Staining for HLA-ABC confirms that U343MG is MHC-$I^{Hi}$, while U87MG is MHC-$I^{Lo}$

(B) Non-targeted LC/MS-MS quantitation of the tumor proteome reveals that U343MG has higher overall protein quantities of HLA-A, -B and -C, compared to U87MG (HLA-A: U343MG vs U87MG 4.67 x $10^7$ vs 1.33 x $10^7$, HLA-B: 2.85 x $10^7$ vs 3.22 x $10^5$, HLA-C: 2.75 x $10^7$ vs 1.13 x $10^7$). These findings were in keeping with our flow cytometric analysis in (A) and provides validation for our detection method for HLA-A, -B, -C in tumors.

(C) Analysis of HLA-A protein quantitation via non-targeted LC-MS/MS finds variable amounts in intervention cases. However, we observed elevated HLA-A quantitation in case 1007 (arrow), which was also the case that highest intratumoral uptake of evolocumab (Median HLA-A quantitation in ID: 1007 of 1.09 x $10^8$ (SD±1.41 x $10^7$) vs control HLA-A quantitation of 2.97 x $10^8$ (SD±2.71 x $10^7$)).

(D) Similarly, HLA-B protein quantitation via non-targeted LC-MS/MS is variable in intervention cases. Again, elevated HLA-B quantitation was observed in case 1007. (Median HLA-B quantitation in ID: 1007 of 3.81 x $10^7$ (SD±5.36 x $10^6$) vs control HLA-B quantitation of 7.69 x $10^6$ (SD±1.29 x $10^7$)).

(E) No discernible difference in HLA-C quantitation was observed between intervention cases or when compared against control untreated samples.

(F) A positive, but non-significant, correlation was observed between intratumoral levels of evolocumab and HLA-A ($R^2$=0.5002, p=0.2928)

(G) Similarly, a positive, but non-significant, correlation was observed between intratumoral levels of evolocumab and HLA-B ($R^2$=0.7269, p=0.1474)

(H) No trend was discernible when comparing intratumoral levels of evolocumab with HLA-C ($R^2$=0.05003, p=0.7763)

(I) Evaluation of Apolipoprotein E levels across intervention and control samples found that lowest levels were seen in the case with highest evolocumab uptake (no treatment mean ApoE quantitation of 6.55 x $10^7$ vs 1007 mean quantitation of 2.97 x $10^7$).

(J) Correlation analysis finds a significant negative trend between ApoE and intratumoral evolocumab ($R^2$=0.9113, p=0.0454*).

Data presented as mean ± SD unless otherwise specified. Correlation analyses were performed using Pearson's Correlation Coefficient (PCC).

**Fig. 6. Increased CD8$^+$ T cell infiltration and MHC-I cell surface expression is observed in tumor tissue with higher evolocumab detection**

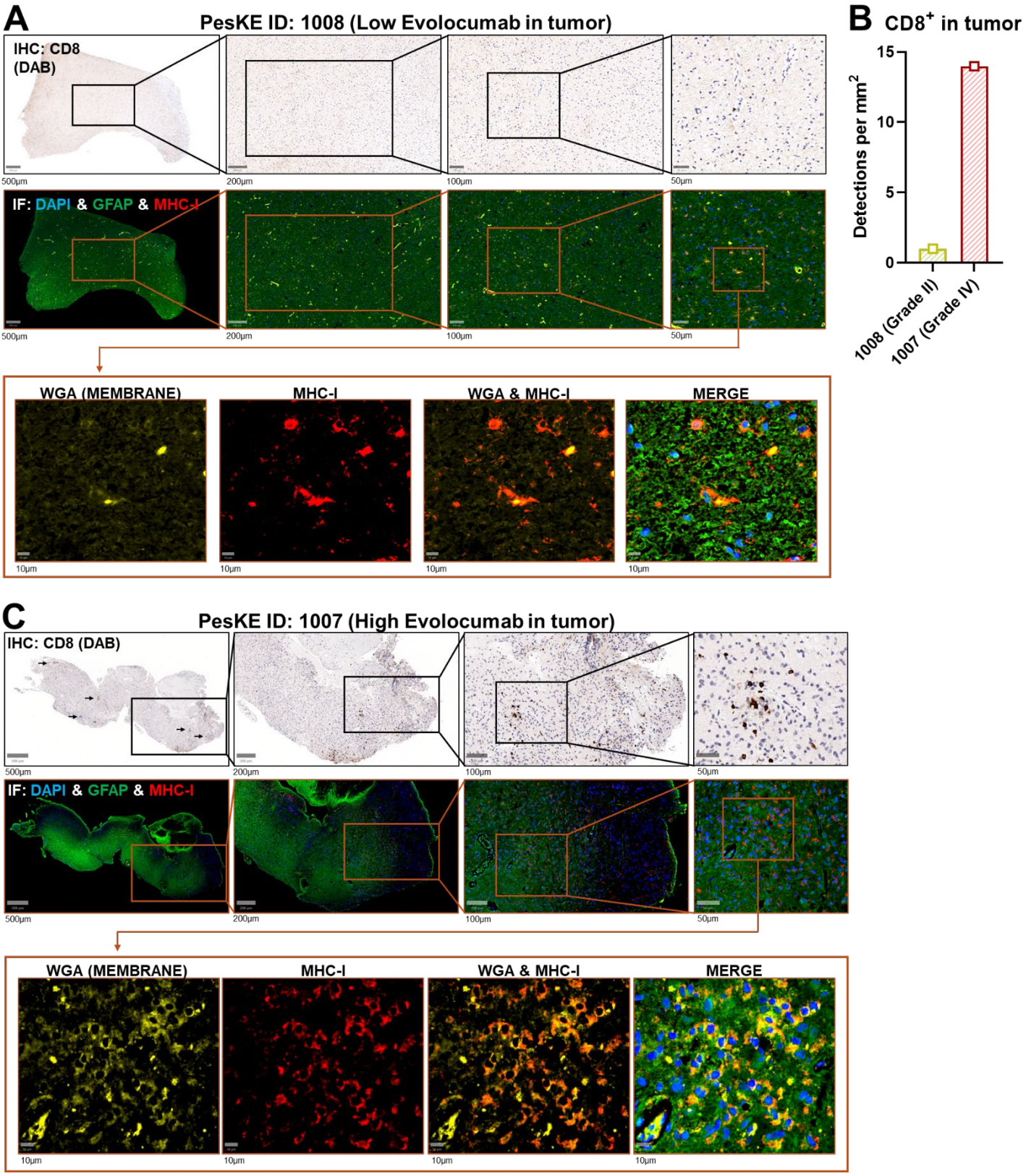

**Fig. 6. Increased CD8+ T cell infiltration and MHC-I cell surface expression is observed in tumor tissue with higher evolocumab detection**

(A) Paired Immunohistochemistry (IHC) and Immunofluorescence (IF) from tissue samples from a case with low evolocumab uptake (ID: 1008, grade II astrocytoma). Limited $CD8^+$ infiltration is observed on IHC staining. IF staining of glial fibrillary acidic protein (GFAP, green), 4',6-diamidino-2-phenylindole (DAPI, nuclei, blue) and MHC-I (red) shows limited MHC-I expression in this tumor. Staining with wheat germ agglutinin (WGA, yellow) to highlight membranes demonstrates limited MHC-I and limited co-localization of MHC-I to cell membranes.

(B) Tumor tissue with lower evolocumab uptake demonstrated lower $CD8^+$ density compared to tissue with higher uptake as assessed via IHC, 1008: 0.9986 $CD8^+$ per $mm^2$ vs 1007: 13.9757 $CD8^+$ per $mm^2$.

(C) IHC staining of tumor tissue from cases with the highest intratumoral evolocumab uptake (ID: 1007, grade IV glioblastoma) reveals multiple areas of inflammatory infiltrate within the parenchyma. Paired IF staining for MHC-I found increased expression in tumor regions which co-localized with areas of $CD8^+$ infiltrate. Co-staining with WGA revealed overlapping MHC-I and WGA expression, suggesting increased membranous MHC-I in tumors with higher evolocumab uptake.

**Fig. 7. Selecting appropriate controls for tissue-based studies**

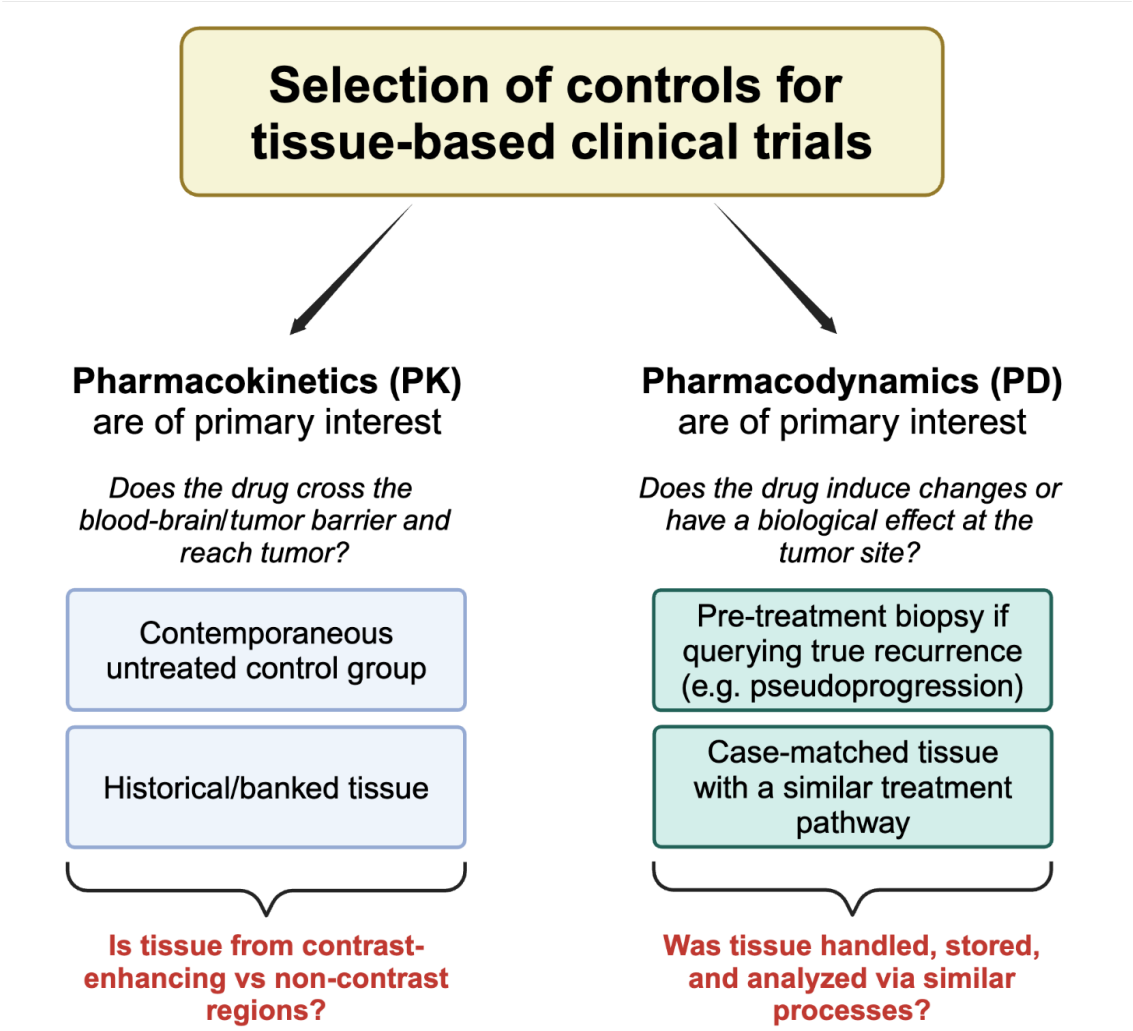

## Table 1. Demographics of consented participants

| **Age at Consent** | **N** | **Mean** | **Std Dev** | **Min** | **Median** | **Max** |
|---|---|---|---|---|---|---|
| Control | 26 | 51.85 | 16.07 | 28.00 | 49.00 | 79.00 |
| Evolocumab | 6 | 53.00 | 19.88 | 28.00 | 52.00 | 74.00 |

| | **Study Group** | | | | **Total** | |
|---|---|---|---|---|---|---|
| | **Control** | | **Evolocumab** | | | |
| | **N** | **%** | **N** | **%** | **N** | **%** |
| **Gender** | | | | | | |
| Male | 12 | 46.15 | 4 | 66.67 | 16 | 50.00 |
| Female | 14 | 53.85 | 2 | 33.33 | 16 | 50.00 |
| **Ethnicity** | | | | | | |
| Not Hispanic or Latino | 25 | 96.15 | 6 | 100.00 | 31 | 96.88 |
| Unknown | 1 | 3.85 | 0 | 0.00 | 1 | 3.13 |
| **Race** | | | | | | |
| White | 22 | 84.62 | 6 | 100.00 | 28 | 87.50 |
| Black or African American | 3 | 11.54 | 0 | 0.00 | 3 | 9.38 |
| Unknown | 1 | 3.85 | 0 | 0.00 | 1 | 3.13 |
| American Indian or Alaska Native | 0 | 0.00 | 0 | 0.00 | 0 | 0.00 |
| Asian | 0 | 0.00 | 0 | 0.00 | 0 | 0.00 |
| Native Hawaiian or other Pacific Islander | 0 | 0.00 | 0 | 0.00 | 0 | 0.00 |
| Not Reported | 0 | 0.00 | 0 | 0.00 | 0 | 0.00 |
| Multi-Race | 0 | 0.00 | 0 | 0.00 | 0 | 0.00 |
| **Histologic Grade** | | | | | | |
| 4 | 18 | 69.23 | 2 | 33.33 | 20 | 62.50 |
| Not Applicable | 6 | 23.08 | 2 | 33.33 | 8 | 25.00 |
| No tumor tissue analysis | 0 | 0.00 | 2 | 33.33 | 2 | 6.25 |
| 3 | 2 | 7.69 | 0 | 0.00 | 2 | 6.25 |
| **Surgical Pathology Diagnosis of Analyzed Sample** | | | | | | |
| Glioblastoma | 17 | 65.38 | 2 | 33.33 | 19 | 59.38 |
| Oligodendroglioma | 3 | 11.54 | 1 | 16.67 | 4 | 12.50 |
| No tumor tissue analysis | 0 | 0.00 | 2 | 33.33 | 2 | 6.25 |
| High Grade Astrocytoma, NOS | 2 | 7.69 | 0 | 0.00 | 2 | 6.25 |
| Low grade astrocytoma, NOS | 0 | 0.00 | 1 | 16.67 | 1 | 3.13 |
| Fibrillary Astrocytoma | 1 | 3.85 | 0 | 0.00 | 1 | 3.13 |

| | | | | | | |
|---|---|---|---|---|---|---|
| Other, specify: High grade glioma | 1 | 3.85 | 0 | 0.00 | 1 | 3.13 |
| Anaplastic Astrocytoma | 1 | 3.85 | 0 | 0.00 | 1 | 3.13 |
| Diffuse Astrocytoma | 1 | 3.85 | 0 | 0.00 | 1 | 3.13 |
| **Disease Status** | | | | | | |
| Newly Diagnosed | 16 | 61.54 | 1 | 16.67 | 17 | 53.13 |
| Previously Treated with Recurrent Disease | 9 | 34.62 | 3 | 50.00 | 12 | 37.50 |
| No tumor tissue analysis | 0 | 0.00 | 2 | 33.33 | 2 | 6.25 |
| Low grade treated, transformed | 1 | 3.85 | 0 | 0.00 | 1 | 3.13 |
| **Disease Description** | | | | | | |
| Unifocal | 24 | 92.31 | 4 | 66.67 | 28 | 87.50 |
| No tumor tissue analysis | 0 | 0.00 | 2 | 33.33 | 2 | 6.25 |
| Multifocal | 1 | 3.85 | 0 | 0.00 | 1 | 3.13 |
| Unknown | 1 | 3.85 | 0 | 0.00 | 1 | 3.13 |
| **Site of Surgical Pathology Tumor** | | | | | | |
| Frontal lobe | 10 | 38.46 | 1 | 16.67 | 11 | 34.38 |
| Temporal lobe | 8 | 30.77 | 0 | 0.00 | 8 | 25.00 |
| Parietal lobe | 5 | 19.23 | 0 | 0.00 | 5 | 15.63 |
| No tumor tissue analysis | 0 | 0.00 | 2 | 33.33 | 2 | 6.25 |
| Frontal-Parietal | 1 | 3.85 | 1 | 16.67 | 2 | 6.25 |
| Temporal-Occipital | 0 | 0.00 | 1 | 16.67 | 1 | 3.13 |
| Frontal-Temporal | 0 | 0.00 | 1 | 16.67 | 1 | 3.13 |
| Insula | 1 | 3.85 | 0 | 0.00 | 1 | 3.13 |
| Parietal-Temporal | 1 | 3.85 | 0 | 0.00 | 1 | 3.13 |
| **Total** | **26** | **100.00** | **6** | **100.00** | **32** | **100.00** |

***NOTE**: Although 6 patients enrolled in the evolocumab group, only 4 had both tumor tissue and blood collected on study.

## Table 2. Toxicity summary of all Adverse Events among participants treated with evolocumab

| | Grade of Adverse Event | | | | | | | | | | |
|---|---|---|---|---|---|---|---|---|---|---|---|
| | 1- Mild | | 2- Mod | | 3-Severe | | 4-LifeThr | | 5-Lethal | | Treated Total |
| | n | (%) | n | (%) | n | (%) | n | (%) | n | (%) | N |
| **Non-Hematologic Adverse Events** | | | | | | | | | | | |
| GASTROINTESTINAL DISORDERS | | | | | | | | | | | |
| Gastritis | 0 | *(0%)* | 1 | *(17%)* | 0 | *(0%)* | 0 | *(0%)* | 0 | *(0%)* | 6 |
| GENERAL DISORDERS AND ADMINISTRATION SITE CONDITIONS | | | | | | | | | | | |
| Injection site reaction | 2 | *(33%)* | 0 | *(0%)* | 0 | *(0%)* | 0 | *(0%)* | 0 | *(0%)* | 6 |
| INFECTIONS AND INFESTATIONS | | | | | | | | | | | |
| Thrush | 1 | *(17%)* | 0 | *(0%)* | 0 | *(0%)* | 0 | *(0%)* | 0 | *(0%)* | 6 |
| METABOLISM AND NUTRITION DISORDERS | | | | | | | | | | | |
| Dehydration | 1 | *(17%)* | 0 | *(0%)* | 0 | *(0%)* | 0 | *(0%)* | 0 | *(0%)* | 6 |
| NERVOUS SYSTEM DISORDERS | | | | | | | | | | | |
| Seizure | 1 | *(17%)* | 0 | *(0%)* | 0 | *(0%)* | 0 | *(0%)* | 0 | *(0%)* | 6 |
| **Non-Hematologic Adverse Events** | | | | | | | | | | | |
| Summary | | | | | | | | | | | |
| **Maximum Non-Hematologic AE** | **4** | ***(67%)*** | **1** | ***(17%)*** | **0** | ***(0%)*** | **0** | ***(0%)*** | **0** | ***(0%)*** | **6** |
| **All Adverse Events** | | | | | | | | | | | |
| Summary | | | | | | | | | | | |
| **Maximum Overall AE** | **4** | ***(67%)*** | **1** | ***(17%)*** | **0** | ***(0%)*** | **0** | ***(0%)*** | **0** | ***(0%)*** | **6** |

**Table 3. Toxicity summary of Adverse Events among participants possibly, probably, or definitely related to evolocumab**

| | Grade of Adverse Event | | | | | | | | | | |
|---|---|---|---|---|---|---|---|---|---|---|---|
| | 1- Mild | | 2- Mod | | 3-Severe | | 4-LifeThr | | 5-Lethal | | Treated Total |
| | n | (%) | n | (%) | n | (%) | n | (%) | n | (%) | N |
| **Non-Hematologic Adverse Events** | | | | | | | | | | | |
| GENERAL DISORDERS AND ADMINISTRATION SITE CONDITIONS | | | | | | | | | | | |
| Injection site reaction | 2 | *(33%)* | 0 | *(0%)* | 0 | *(0%)* | 0 | *(0%)* | 0 | *(0%)* | 6 |
| **Non-Hematologic Adverse Events** | | | | | | | | | | | |
| Summary | | | | | | | | | | | |
| **Maximum Non-Hematologic AE** | **2** | ***(33%)*** | **0** | ***(0%)*** | **0** | ***(0%)*** | **0** | ***(0%)*** | **0** | ***(0%)*** | **6** |
| **All Adverse Events** | | | | | | | | | | | |
| Summary | | | | | | | | | | | |
| **Maximum Overall AE** | **2** | ***(33%)*** | **0** | ***(0%)*** | **0** | ***(0%)*** | **0** | ***(0%)*** | **0** | ***(0%)*** | **6** |

# Supplementary Materials:

**List: Fig. S1. to S2.** Mechanism of PCSK9i for increasing surface MHC-I and study schema. No SM specific references.

## Fig. S1. Mechanism of PCSK9 inhibition on increasing MHC-I expression

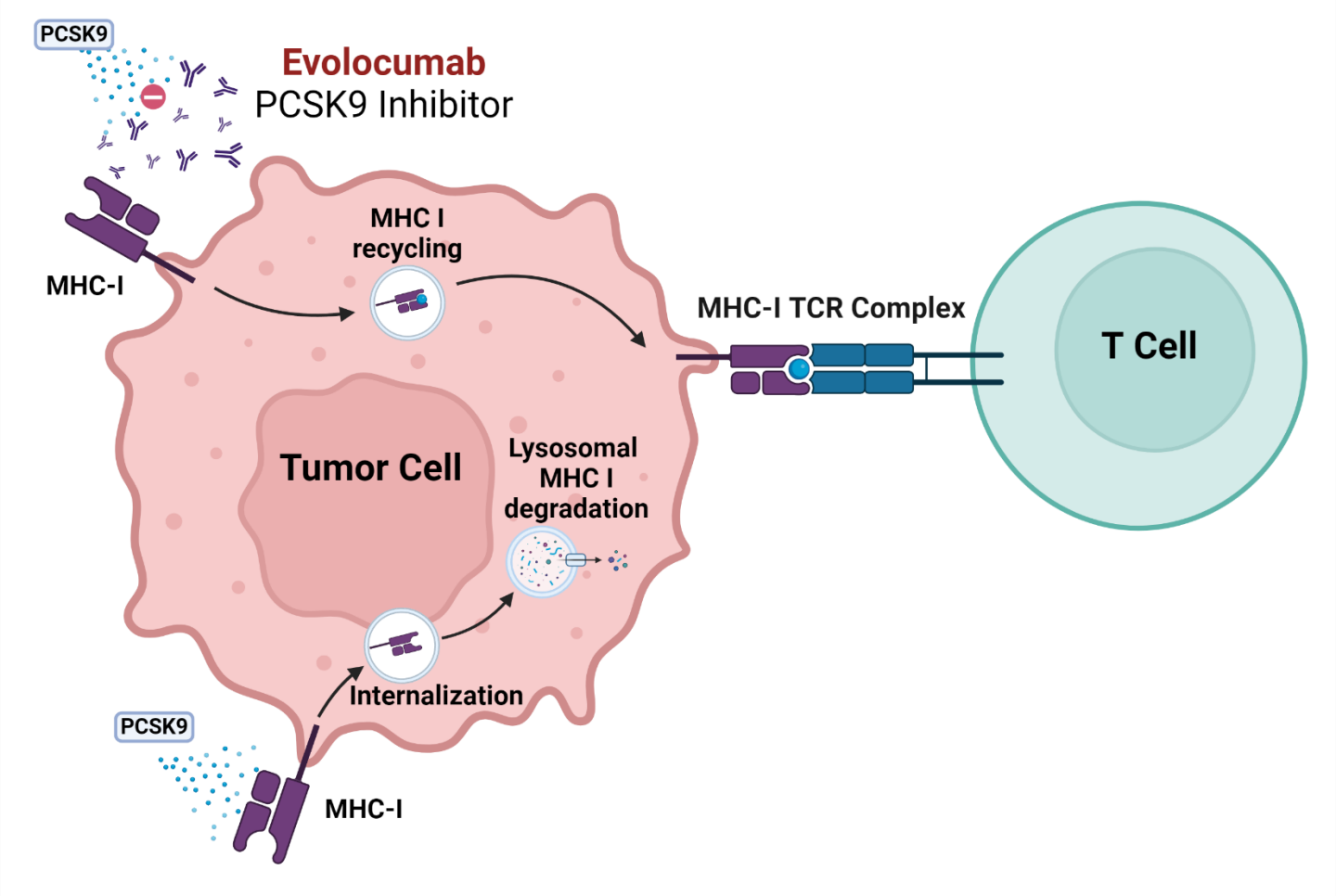


PCSK9 associates with MHC-I and promotes its degradation within intracellular lysosomes. Evolocumab inhibits PCSK9 by binding it and preventing it interacting with surface receptors such as MHC-I. MHC-I is instead recycled back to the cell surface, where it can present neoantigens to $CD8^+$ lymphocytes. Created with BioRender.com.

**Fig. S2. Trial Design**